First-principles study of Pb_2MgTeO_6: High-T cubic phase and average low-T rhombohedral phase

Razvan Caracas and Xavier Gonze
Université Catholique de Louvain, Unité de Physico-Chimie et de Physique de Matériaux, pl. Croix du Sud 1, B-1348 Louvain-la-Neuve, Belgium
(Received 17 October 2001; published 23 April 2002)

The Pb_2MgTeO_6 double perovskite is cubic at high temperature and becomes incommensurately modulated with a rhombohedral $R\bar{3}$ average structure at lower temperatures. Both the cubic and rhombohedral average structures are investigated using the local-density approximation within the density-functional theory: We determine the electronic, structural, dielectric, and zone-center dynamical properties. The computed structural parameters are in reasonable agreement with the experiment, with differences up to 2% for the lattice constants. There are two unstable zone-center vibration modes in the cubic phase. The first unstable mode T_{1g}, $91.19i$ cm^{-1}, has an antiferrodistortive character, while the second, T_{1u}, $13.92i$ cm^{-1}, has a ferrodistortive character. There is no unstable zone-center mode in the rhombohedral phase. We establish the correspondence between the zone-center modes in the two phases.

DOI: 10.1103/PhysRevB.65.184103 PACS number(s): 78.20.Ci, 71.20.−b, 78.30.−j, 61.44.Fw

I. INTRODUCTION

Incommensurate (IC) phases occur when a periodic structure is subject to a spatially periodic modulation whose wavelength is incommensurate with respect to the basic underlying lattice. There are more than 130 inorganic IC compounds[1–6] where the modulation has a displacive and/or occupational character. For most of these compounds the mechanisms governing the phase transitions leading to IC structures are unknown, except for metals, in which case the formation of a charge density wave is often invoked.[7]

Among perovskitelike oxides, the presence of an incommensurate modulation is a very unusual phenomenon. Up to now just a few such perovskites have presented an incommensurate phase: Pb_2CoWO_6,[8] Pb_2CdWO_6,[9] $PbSc_{1/2}Ta_{1/2}O_3$,[10] and Pb_2MgTeO_6.[11,12] In all these compounds incommensurability was discovered recently. Out of all these materials Pb_2MgTeO_6 presents some remarkable properties: (i) the temperature range of existence of the IC phase is very large, down to 0 K; (ii) it does not have a lock-in transition (blocking of the modulation wavevector to a commensurate value, generating a commensurate structure); and (iii) the cations are well ordered.

This material is face-centered-cubic at high temperature (phase I) and it transforms at 194 K to a first IC-modulated rhombohedral structure (phase II) and at 142 K to another IC-modulated rhombohedral structure (phase III). The rhombohedral structures may be derived from the cubic high-T structure by applying small distortions.

In view of the theoretical understanding of the mechanisms responsible for the incommensurate phase transitions, the structure and the properties of Pb_2MgTeO_6 are particularly attractive. Moreover, its average structure is highly symmetric, with just a few atoms in the unit cell.

In the framework of the local-density approximation (LDA) within the density functional theory (DFT),[13,14] we determined the electronic, structural and zone-center dynamical properties of both the cubic high-T phase I and the *average* structure of the low-T phase III as a first step in the analysis of the incommensurate phase.

We find that Pb_2MgTeO_6 is an insulator with a large LDA electronic gap (about 3 eV). The electronic band structure is made of weakly dispersive bands. The deviations between the *ab initio* determined structure and the experimental structure are more important for the rhombohedral phase (up to 2% in lattice constants and up to 8.5% in bond lengths) than for the cubic phase (up to 2% in lattice constants and up to 3.5% in bond lengths). However, the deviations in bond lengths for the rhombohedral phase are within the range of distances allowed by the modulation. The calculated Born effective charges are not too different from the nominal charges. The rhombohedral phase does not present any instability in the Γ point, while in the cubic phase we find two unstable modes (one T_{1g} mode, $91.19i$ cm^{-1}, and one T_{1u} mode, $13.92i$ cm^{-1}). Both these modes may be responsible for phase transitions leading to rhombohedral phases.

The paper is organized as follows. Details of the calculation methods are presented in Sec. II. Section III presents the crystal structures of the two considered polymorphs. Section IV describes the electronic properties, and Sec. V presents the theoretical determination of the structure. The dielectric properties are discussed in Sec. VI, while the phonons at the Γ point are analyzed in Sec. VII. The paper will end with the conclusions.

II. COMPUTATIONAL DETAILS

All the calculations are based on the LDA of the DFT.[13,14] We use the ABINIT code, a common project of the Université Catholique de Louvain, Corning Incorporated and other contributors (ABINITV2.X, 1999-2000,[15]). The ABINIT software is based on pseudopotentials and plane waves. It relies on the adaptation to a fixed potential of the band-by-band conjugate gradient method[16] and on a potential-based conjugate-gradient algorithm for the determination of the self-consistent potential.[17] The wave functions describe only the outer electrons, while the core electrons are taken into ac-

count using pseudopotentials. We use Troullier-Martins pseudopotentials[18] for Mg, Te, and O and an extended Teter norm-conserving pseudopotentials[19] for Pb. The considered valence electrons for Pb, Mg, Te, and O are $5d^{10}6s^26p^2$, $3s^2$, $5s^25p^4$, and $2s^22p^4$, respectively. All the calculations are performed at 0 K.

For the characterization of the electronic properties, a set of convergence tests was performed in order to choose correctly the grid of special k points[20] and the cutoff for the plane-wave kinetic energy. During these tests the k-point grid density and the plane-wave cutoff kinetic energy were consecutively and independently increased. The variation of the total energy was monitored. A difference of 1 m Hartree (1 Hartree $=27.211$ eV) between two successive grids or cutoff energies was considered indicative of sufficient convergence. A grid of 32 special k points in the full Brillouin zone (Monkhorst-Pack $4\times4\times4$), folding to six points and to two points in the irreducible part of the Brillouin zone of the rhombohedral and cubic structures, respectively, and a plane-wave kinetic energy cutoff of 26 Hartree were finally adopted for the calculation of the electronic properties. The determination of the crystal structure and the dynamical properties needed separate convergence tests of the density of the grid of k points (see below).

The structural relaxation was conducted using the Broyden-Fletcher-Goldfarb-Shanno (BFGS) minimization, modified to take into account the total energy as well as the gradients (as in usual BFGS minimization).[21]

Several increasing k-point grids were used in order to ensure the convergence of the structural parameters. The results of each k-point grid were tested in the next denser grid and the residual stresses and the cartesian forces were monitored. A value of the stresses of less than 5.0×10^{-5} Hartree/bohr^3 and a value of forces of less than 1.0^{-4} Hartree/bohr were considered sufficiently accurate. The same grid of k points (Monkhorst-Pack $4\times4\times4$) was enough to attain the desired convergence.

Technical details on the computation of responses to atomic displacements and homogeneous electric fields can be found in Ref. 22, while Ref. 23 presents the subsequent computation of dynamical matrices, Born effective charges, dielectric permittivity tensors, and interatomic force constants.

III. CRYSTAL STRUCTURE

In Pb_2MgTeO_6 the high-temperature phase I has a double ABO_3 perovskite-type structure, rocksalt-ordered[24,25] (Fig. 1). It is cubic-face-centered, with ten atoms in the primitive unit cell.

The Pb atoms are situated in the middle of the octants of the conventional unit cell, with reduced positions (1/4 1/4 1/4), while the Mg and Te cations are situated on the corners (0 0 0) and on the middle of the cubic edges (1/2 0 0) respectively. The O atoms are situated between the Mg and Te cations, slightly displaced from the middle of the Mg-Te toward the Te atoms in positions (0.26 0 0).[12] Thus there are alternances of the cations like Mg-O-Te-O-Mg and Mg-Pb-Te-Pb-Mg along the cubic [100] and [111] directions, respectively.

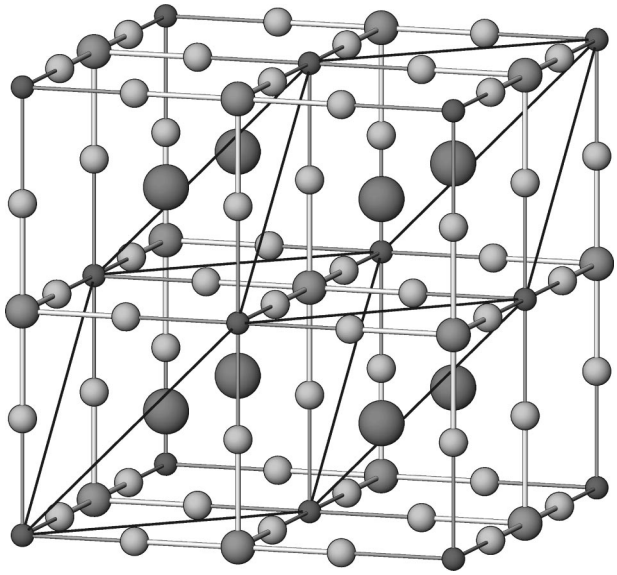

FIG. 1. The structure of the high-T cubic phase of Pb_2MgTeO_6. The spheres represent, in order of decreasing size, Pb, Te, O, and Mg.

The cubic phase transforms at 192 K to a first incommensurate phase II with space group of the average structure $R\bar{3}m$. The existence of this phase and the transition temperature have been determined experimentally using electron microscopy, x-ray diffraction, calorimetric, dielectric, and polarization measurements.[11] The symmetry has been deduced on the group-subgroup relationships. This rhombohedral structure is incommensurately modulated with a modulation wave vector $(\delta\delta\delta)$. The experimental determination of the lattice constants and the internal coordinates has not been performed yet.

This phase transforms to another low-temperature rhombohedral phase III at 142 K. This latter phase has symmetry $R\bar{3}$ and it is also incommensurately modulated with a modulation wave vector $(\delta\delta\delta)$, where δ is close to 0.1066 at 6 K.[12] This structure has been experimentally determined by a Rietveld refinement of neutron powder diffraction data.

The rhombohedral structure of phase III is obtained from the cubic one by squeezing the primitive cubic unit cell. According to the experimental results, the rhombohedral angle changes from $\alpha=60.0°$ for the primitive cubic lattice to $\alpha=59.9°$. The experimental lattice constants are the same as for the primitive cubic lattice. Both the O and Pb atoms are displaced from their positions in the cubic structure. The O atoms which lie on the Mg-O-Te-O directions in the cubic structure move closer to the diagonal threefold rotation axis. The Pb atoms are also slightly displaced from their original cubic positions away from the diagonal axis. They may randomly occupy one of the three equivalent positions obtained after this displacement. However we approximate the Pb positions as (1/4 1/4 1/4) for both the cubic and rhombohedral structures because, according to experimental data, the incommensurability affects mainly the O atoms and not the Pb atoms.[26]

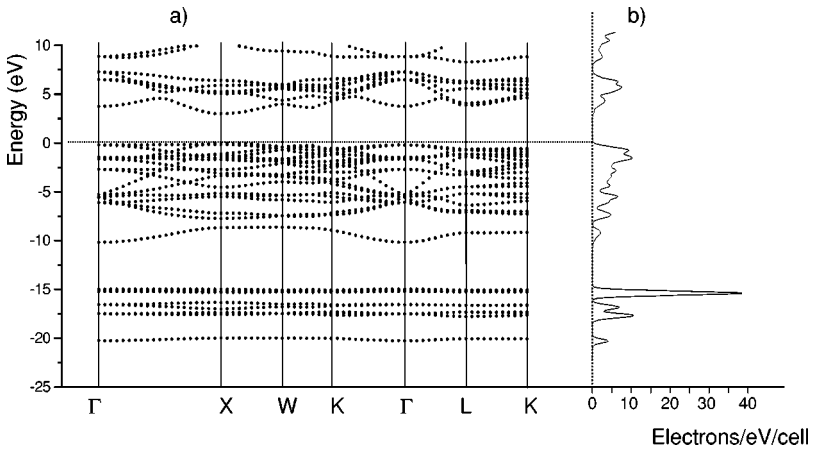

FIG. 2. The electronic band structure (a) and the corresponding density of states (DOS) (b) in phase I of Pb_2MgTeO_6. The bands are weakly dispersive, with O*s* contributions in the low-energy zone of the valence bands and O*p* contributions in the high-energy zone of the valence energy bands.

IV. ELECTRONIC PROPERTIES

We start our study with a determination of the ground-state properties, to have a basis for treating later the dynamical properties. The analysis of the valence charge density reveals the main features of the chemical bonds and the ionization of the atoms. It is rather independent of the starting geometry. The Pb atoms almost completely lose their 6*p* electrons, while keeping their 5*d* electrons. The 6*s* electrons participate in the weak covalent bonds with the surrounding O atoms. The Mg atoms are highly ionized, losing all their valence electrons to the oxygens. The Te atoms preserve some of their 5*s* and 5*p* electrons which participate to covalent bonds with the coordinating oxygens. The additional electrons belonging to the oxygens are localized along the Mg-O-Te bond directions. The electronic band structure and the corresponding electronic density of states (DOS) are almost identical for both the cubic, high-*T* phase I and the rhombohedral, low-*T* phase III.

The valence electronic bands are weakly dispersive (Fig. 2). Along the Γ-*X*, Γ-*K*, and Γ-*L* lines the bands are more dispersive than along lines like *X*-*W*, *W*-*K*, or *K*-*L*, where all the bands are almost flat. The O*s* electrons dominate the lower valence bands and the O*p* dominate the higher valence bands. Different other electrons from the Pb and Te cations participate to the lower valence bands.

The first peak in the DOS (about -20 eV) is assigned to O*s* and Te hybrids and the next, double, peak (about -18 and -17 eV) to O*s* and Pb hybrids. They both have a bonding character, the corresponding electronic charge density being polarized along the bonds. The Pb 5*d* orbitals are situated higher in energy than the O 2*s* orbitals. They form flat bands corresponding to a sharp peak in the DOS (about -15 eV). The rest of the Te electrons, together with O*p* and O*s* hybridized orbitals, form an isolated band in the intermediate range of energy (about -10 eV). The O*p* electrons are responsible for the other valence bands. They are more dispersive than the low-energy valence bands, and the corresponding electronic orbitals are highly hybridized. They have first a bonding character, while increasing in energy the antibonding character is accentuated.

Pb_2MgTeO_6 presents a large LDA electronic gap of about 2.6 eV, direct in *X*. The first conduction bands have an antibonding character. Their electronic charge stems from O*p* and Te orbitals. Higher in energy we find other Te+O hybrids and O*p* orbitals.

V. AB INITIO STRUCTURAL DETERMINATION

The theoretical results of the structural relaxation are summarized in Table I for the cubic phase and in Table II for the rhombohedral phase. The lattice constants for both the $Fm\bar{3}m$ and $R\bar{3}$ phases are slightly underestimated (-2%) with respect to the experimental values. We observe that within the experimental uncertainty, the primitive cubic and rhombohedral lattice constants are equal. Our calculations give smaller values than the experiment for both, with a tiny difference between them, less than 0.2%. The α angle of the rhombohedral structure is slightly overestimated. This overestimation stems from a compression, rather than the experimental extension, of the initial cubic lattice along a diagonal threefold axis.

All the theoretical values of the interatomic bond distances in the cubic phase are smaller than the experimental values (up to 3.5–3.7 % discrepancy). The underestimation of the volume of the TeO_6 octahedra is larger than the underestimation of the MgO_6 octahedral volume, while for the PbO_{12} polyhedra the deviation is extremely small.

In case of the rhombohedral phase at 0 K, the experimental structure is incommensurately modulated. Consequently there is a large spread of the experimental bond distances around the mean values (corresponding to the average structure) within some continuous intervals.[27] In the following we will first make comparisons with the average values for the interatomic distances, and then we will see the position of

TABLE I. Cubic phase: *ab initio* structural determination and comparison with the experiment.

Parameter	Theory	Expt. (Ref. 12)	Diff.
a_0 (Å)	7.833	7.984	-1.89 %
O*x*	0.2645	0.2600	0.0045
Mg-O bond (Å)	2.072	2.081	-0.43 %
Te-O bond (Å)	1.844	1.911	-3.50 %
Pb-O bond (Å)	2.608	2.709	-3.78 %
O-O bond (Å)	2.930	2.935	-0.17 %

TABLE II. Rhombohedral phase: *ab initio* structural determination and comparison with the experiment. We present first the theoretical results, then the range of values obtained in the real incommensurate structure and their average. Next we compare our theoretical results with the average values. The last column gives the spread in the IC structure relative to the average.

Parameter	Theory	Expt. IC (Ref. 12)	Expt. average (Ref. 12)	Diff.	Spread
a_0 (Å)	5.531		5.645	-2.01 %	
α(°)	60.27		59.9	0.37°	
Ox	0.2669	0.1965–0.3050	0.2408	0.0261	0.1085
Oy	0.7646	0.6828–0.7726	0.7384	0.0262	0.0898
Oz	0.7051	0.7356–0.7788	0.7559	-0.0508	0.0432
Pbx	0.2507	0.2320–0.2680	0.2500	0.0007	0.036
Mg-O bond (Å)	2.084	1.910–2.172	2.029	2.71 %	12.91 %
Te-O bond (Å)	1.848	1.833–2.106	1.983	-6.80 %	13.77 %
Pb-O bond (Å)	2.776	2.409–3.236	2.831	-1.93 %	29.21 %
O-O bond (Å) [a]	2.968	2.452–3.262 [b]	2.783	6.64 %	29.11 %
O-O bond (Å) [a]	2.928		2.924	0.13 %	27.70 %
O-O bond (Å) [c]	2.614		2.855	-8.44 %	28.37 %
O-O bond (Å) [c]	2.612		2.724	-4.11 %	29.74 %

[a]In MgO_6 octahedra.
[b]Global spreading for all O-O bonds.
[c]In TeO_6 octahedra.

our results within the continous intervals.

In the rhombohedral phase III, the deviations between the calculated and the average experimental bond lengths are greater than in the cubic phase I. Thus the calculated Mg-O bond lengths are slightly larger (+2.71%) than the average experimental values, while the calculated Te-O bond lengths are much smaller (-6.8%) than the experimental average values. The Pb-O bond lengths are just slightly smaller (-1.93%) than the experimental ones. The two O-O unequivalent bond distances for the oxygens belonging to the Mg-centered octahedra are larger (+0.1% and +6.6%) in our calculations than the mean experimental values. Furthermore the two unequivalent bonds between the oxygens belonging to the Te-centered octahedra are smaller (-4.1% and 8.4%) than the experimental data. Thus our calculations tend to increase the volume of the MgO_6 octahedra while decreasing the volume of the TeO_6 octahedra, if we take the mean values as reference.

However, the spread in the experimental bond distances accounts for variation of up to 15% from the average value. Consequently, we see that the deviations of the theoretical results with respect to the mean bond length values are all smaller than the spread of the bond lengths in the IC structure and that all our results fall close to the middle of the continous intervals of existence of the real bonds.

All the calculated cation-oxygen bond distances are larger in the rhombohedral phase III than in the cubic phase I. With the exception of the Mg-O bond distance the same trend is observed when comparing the experimental data. The distances between the oxygens behave rather differently. All the experimental values for the rhombohedral structure are smaller than those for the cubic one. According to our calculations there is one exception for one of the two O-O distances between the oxygens belonging to the MgO_6 octahedra.

VI. DIELECTRIC PROPERTIES

The determination of the dielectric properties plays an important role in the calculation of the long-range interatomic forces. For the cubic phase we obtained an electronic dielectric constant ϵ^{∞} of 5.44, which corresponds to a refractive index of 2.33. The rhombohedral phase presents slightly smaller values $\epsilon^{\infty}_{11}=5.36$, $\epsilon^{\infty}_{22}=5.36$, and $\epsilon^{\infty}_{33}=5.32$, corresponding to a refractive index of [2.31 2.31 2.30]. The computed static dielectric constant ϵ_0 for the rhombohedral phase is [80.1 80.1 226.8]. The anisotropy in the static dielectric tensor is due to the different LO-TO splitting between the A_u and E_u soft modes. We are not aware of published experimental data.

We further computed the Born effective charges, defined as the change in polarization due to an atomic displacement under zero external electric field, see Table III. The Pb effective charge is higher than the nominal charge of the Pb^{2+}

TABLE III. Computed Born effective charges for the phases I and III of the PMT. The eigenvalues of the charge tensors and the nominal charges are presented. The considered reference system for the charge tensors is the Cartesian one, parallel to the primitive cubic cell, for both phases. The rhombohedral phase cell is oriented such as the rhombohedral [111] direction is the same as the cubic [100] direction, and the rhombohedral [100] direction is contained in the (010) cubic plane.

Element	Phase I	Phase III	Nominal charges
Pb	3.938	[3.873 3.873 3.842]	2
Mg	2.436	[2.462 2.462 2.415]	2
Te	4.486	[4.503 4.503 4.576]	6
O	[-2.462 -2.462 -2.463]	[-2.324 -2.440 -2.569]	-2

TABLE IV. Calculated and experimental phonon frequencies at the Γ point in the cubic phase I in Pb_2MgTeO_6. (Raman active modes only. Other computed mode frequencies are given in the text.)

Mode symmetry	Calc. phonon (cm^{-1})	Experimental value (cm^{-1}) [a]	Diff. (%)
A_{1g}	826.39	759	8.8 %
E_g	641.21	568	12.8 %
T_{1g}	91.19i		
T_{2g}	56.20	58	-3.1 %
	389.65	357	9.1 %

[a]Reference 26.

ion. The Mg effective charge is somewhat larger than the nominal charge of the Mg^{2+} ion. The Te effective charge is smaller than the nominal charge of the Te^{6+} ion. The effective charge of the oxygens is expected to be anisotropic, due to the anisotropy of the environment around the oxygens. But the difference between the three computed diagonal values is extremely small (-2.462, -2.462, and -2.463), and close to the nominal charge of the O^{2-} ions (-2).

For the rhombohedral structure the deviations of the effective charge with respect to the nominal charges are slightly increased. The anisotropy of the oxygen effective charge is accentuated.

These Born effective charges do not follow the trends that have been observed for other ferroelectric perovskites. We remark the absence of large anomalies of the O effective charges [common in perovskites like $BaTiO_3$, $PbTiO_3$,[28,29] or even WO_3 (Ref. 29)]. If in ABO_3 perovskites the anomalous effective charge of O is due to a coupling between the O $2p$ orbitals and the d orbital of the transition-metal B atom,[30–32] in Pb_2MgTeO_6, the B atoms (namely Mg and Te) are not transition-metals, such p-d coupling does not occur and the effective charge of the O atoms is not anomalous. Similarly, the nontransition metal Mg has an effective charge close to the nominal value,[33] and the deviations are more important for the Te and Pb.

VII. DYNAMICAL PROPERTIES

We further computed the vibration modes at the Γ point for both structures. The complete list of the calculated phonons and the experimental Raman and IR modes for the cubic phase I are listed in Table IV and of the calculated phonons for the rhombohedral phase III in Table V. For the cubic phase I, on the basis of group theory, we obtain a decomposition of vibration modes as: $1A_{1g}+1E_g+1T_{1g}+2T_{2g}+4T_{1u}+1T_{2u}$ modes, while for the rhombohedral phase III we obtain $4A_g+4E_g+6A_u+5E_u$ modes. In the following we will make the analysis of the g and u modes first in the cubic phase I, and then in the rhombohedral phase III.

In the cubic phase I, the deviations between the calculated positive g modes and the experimental Raman modes range between -3.1% and 12.8% (Table IV). All the positive high-frequency modes are overestimated, while the low-frequency positive mode is slightly underestimated. There is an unstable g mode, with symmetry T_{1g}, situated at 91.19i cm^{-1}. This mode correspond to a rotation of MgO_6 and TeO_6 octahedra. These rotations are performed around [100] directions, in different sense for MgO_6 octahedra and for TeO_6 octahedra. In each octahedron, the four equatorial oxygens participate to this rotation while the remaining two apical oxygens vibrate inversely and diagonally in (100) planes. The coupling of the three T_{1g} components in Γ generates rotations of the octahedra around the [111] family of axes, that may lead to the phase transition to the $R\bar{3}$ average structure, which has an antiferrodistortive character.

TABLE V. Calculated phonons at the Γ point in the average structure of the rhombohedral phase III in Pb_2MgTeO_6.

Mode symmetry	Calc. phonon (cm^{-1})
A_g	61.13
	125.82
	384.29
	811.58
E_g	37.75
	79.25
	396.68
	627.84
Mode symmmetry	Calc. phonon (TO ; LO) (cm^{-1})
A_u	37.96 ; 151.17
	292.22 ; 310.36
	316.74 ; 363.15
	385.19 ; 482.39
	734.54 ; 776.53
E_u	63.78 ; 153.82
	283.62 ; 285.62
	308.37 ; 365.65
	389.97 ; 493.38
	738.27 ; 779.58

There are six u modes in the cubic phase I: four u modes with T_{1u} symmetry (TO: 13.92i, LO: 150.06 cm^{-1}; TO: 304.19, LO: 372.0 cm^{-1}; TO: 390.88, LO: 484.17 cm^{-1}; and TO: 752.32, LO: 792.56 cm^{-1}), one u mode with T_{2u} symmetry (277.48 cm^{-1}), and three acoustic modes. In the unstable u mode all the atoms are displaced along the [100] directions, the Pb atoms are displaced in the positive direction, and all other atoms are displaced in the negative direction. This mode has been also found in, e.g., $BaTiO_3$,[34] and it may produce a tetragonal distortion or a rhombohedral distortion.

In the rhombohedral phase all the computed vibration modes at the Γ point are positive, indicating the absence of an instability in the center of the Brillouin zone. There are only Raman experimental measurements of phonon frequencies in the IC phase, obtained from a powder material. The character of the samples as well as the presence of the incommensurate modulation (which projects in the zone-center contributions from the n-**q** points) are responsible for the observed broad peaks (several smaller peaks are superposed

onto one central peak). If we compare our results with the values of the main central experimental peaks, the same trend as for the cubic phase is conserved. A detailed analysis of the Raman spectra of the rhombohedral IC phase will be the subject of a further paper.

We now link the high-frequency modes of the cubic structure and the rhombohedral one using symmetry and numerical considerations. In the symmetry lowering from $Fm\bar{3}m$ to $R\bar{3}$, the *u/g* character of the modes is preserved, while the threefold-degenerate *T* modes are split into $A+E$ rhombohedral modes. The 1 or 2 character is lost. The cubic A_{1g} mode (826.39 cm^{-1}) transforms to the rhombohedral A_g mode (811.58 cm^{-1}). The E_g cubic mode (641.21 cm^{-1}) transforms to the rhombohedral E_g mode (627.84 cm^{-1}). The cubic T_{2g} mode (389.65 cm^{-1}) splits into the rhombohedral E_g mode (396.68 cm^{-1}) and the A_g mode (384.29 cm^{-1}). For the *u* modes the assignment of the splitting of the cubic T_{1u} and T_{2u} to the rhombohedral modes E_u+A_u can be done on the basis of the numerical values. The unstable T_{1u} mode in the cubic phase (TO, $13.92i$ cm^{-1}; LO, 150.06 cm^{-1}) splits into E_u (TO, 63.78 cm^{-1}; LO, 153.82 cm^{-1}) and A_u (TO, 37.96 cm^{-1}; LO, 151.17 cm^{-1}) modes. The T_{1u} and T_{2u} modes have nearly the same energy, and mix somehow. The third (fourth, respectively) T_{1u} mode in the cubic phase corresponds to the fourth (and fifth, respectively) A_u and E_u modes.

VIII. CONCLUSIONS

We showed that Pb_2MgTeO_6 is an insulator with a large band gap. The Mg and Pb atoms are ionized, while the Te and O atoms form relatively strong covalent bonds. The theoretical structural determination provided results in reasonable agreement with the experiment for the cubic phase. In the case of the rhombohedral phase the experimental data present continuous intervals of values of interatomic lengths around those corresponding to the average structure. The existence of these intervals is due to the incommensurate modulation. The deviations of our results with respect to the experimental average values are all much smaller than the spread due to the modulation. We observe the absence of anomalies of the O effective charges, which might be due to the fact that the chains Mg-O-Te-O-Mg do not allow the flow of a polarization current. Such a feature usually dominates the physics of Born effective charges for ferroelectric perovskites. The analysis of the phonons in the Γ point reveals the presence of two instabilities in the cubic phase. The first unstable mode, with symmetry T_{1u}, corresponds to a ferroelectric transition, and the second unstable mode, with symmetry T_{1g}, corresponds to an antiferrodistortive transition. Both of them may be responsible for phase transitions leading to rhombohedral phases, but the T_{1g} mode actually freeze-in the $Fm\bar{3}m$-to-$R\bar{3}$ transition. The average rhombohedral phase does not present any zone-center instability.

ACKNOWLEDGMENTS

We thank G. Baldinozzi and Ph. Ghosez for interesting discussions and suggestions. Part of this research was supported by the FRFC project No. 2.4556.99. X.G. acknowledges financial support from the FNRS.

[1] *Incommensurate Phases in Dielectrics*, edited by R. Blinc and A. P. Levanyuk (North-Holland, Amsterdam, 1986).
[2] H. Z. Cummins, Phys. Rep. **185**, 211 (1990).
[3] E. F. Bertaut, Crystallogr. Rev. **2**, 107 (1993).
[4] S. Van Smaalen, Crystallogr. Rev. **4**, 79 (1995).
[5] G. Madariaga, E. Kroumova, and J. A. Luna, http://www.cryst.ehu.es/icsdb/index.html, (2001).
[6] R. Caracas, http://www.mapr.ucl.ac.be/~crystal/, J. Appl. Crystallogr. **35**, 120 (2002).
[7] G. Gruner, *Density Waves in Solids* (Perseus, Cambridge, MA, 1994).
[8] M. Bonin, W. Paciorek, K. Schenk, and G. Chapuis, Acta Crystallogr., Sect. B: Struct. Sci. **51**, 48 (1995).
[9] G. Baldinozzi, G. Calvarin, Ph. Sciau, D. Grebille, and E. Suard, Acta Crystallogr., Sect. B: Struct. Sci. **55**, 1 (1999).
[10] C. A. Randall, S. A. Markgraf, A. S. Bhalla, and K. Baba-Kishi, Phys. Rev. B **40**, 413 (1989).
[11] G. Baldinozzi, Ph. Sciau, and A. Bulou, J. Phys.: Condens. Matter **9**, 10 531 (1997).
[12] G. Baldinozzi, D. Grebille, Ph. Sciau, J.-M. Kiat, J. Moret, and J.-F. Berar, J. Phys. (Paris) **10**, 6461 (1998).
[13] P. Hohenberg and W. Kohn, Phys. Rev. **136**, B864 (1964).
[14] W. Kohn and L. J. Sham, Phys. Rev. **140**, A1133 (1965).
[15] X. Gonze, R. Caracas, P. Sonnet, F. Detraux, P. Ghosez, I. Noiret, and J. Schamps, in *First-Principles Study of Crystals Exhibiting an Incommensurate Phase Transition*, edited by H. Krakauer, AIP Conf. Proc. No. **535** (AIP, Melville, NY, 2000), pp. 13–20.
[16] M. C. Payne, M. P. Teter, D. C. Allan, T. A. Arias, and J. D. Joannopoulos, Rev. Mod. Phys. **64**, 1045 (1992).
[17] X. Gonze, Phys. Rev. B **54**, 4383 (1996).
[18] N. Troullier and J. L. Martins, Phys. Rev. B **43**, 1993 (1991).
[19] M. Teter, Phys. Rev. B **48**, 5031 (1993).
[20] H. J. Monkhorst and J. D. Pack, Phys. Rev. B **13**, 1976 (1976).
[21] W. H. Press, B. P. Flannery, S. A. Teukolsky and W. T. Vetterling, *Numerical Recipes. The Art of Scientific Computing (FORTRAN Version)* (Cambridge University Press, Cambridge, 1989).
[22] X. Gonze, Phys. Rev. B **55**, 10 337 (1997).
[23] X. Gonze and C. Lee, Phys. Rev. B **55**, 10 355 (1997).
[24] L. Bellaiche and D. Vanderbilt, Phys. Rev. Lett. **81**, 1318 (1998).
[25] R. Hemphill, L. Bellaiche, Alberto Garcia, and D. Vanderbilt, Appl. Phys. Lett. **77**, 3642 (2000).
[26] G. Baldinozzi (private communication).
[27] In non-incommensurate alloys, different Pb-O bond lengths can also occur. However, only a few different bonds can be characterized, while the spread is continuous in the present case.
[28] Ph. Ghosez, J.-P. Michenaud, and X. Gonze, Phys. Rev. B **58**, 6224 (1998).
[29] F. Detraux, Ph. Ghosez, and X. Gonze, Phys. Rev. B **56**, 983 (1997).

[30] W. Zhong, R. D. King-Smith, and D. Vanderbilt, Phys. Rev. Lett. **72**, 3618 (1994).
[31] M. Posternak, R. Resta, and A. Baldereschi, Phys. Rev. B **50**, 8911 (1994).
[32] Ph. Ghosez and X. Gonze, J. Phys.: Condens. Matter **12**, 9179 (2000).
[33] L. Bellaiche and D. Vanderbilt, Phys. Rev. Lett. **83**, 1347 (1999).
[34] Ph. Ghosez, E. Cockayne, U. V. Waghmare, and K. M. Rabe, Phys. Rev. B **60**, 836 (1999).